Since January 2020 Elsevier has created a COVID-19 resource centre with free information in English and Mandarin on the novel coronavirus COVID-19. The COVID-19 resource centre is hosted on Elsevier Connect, the company's public news and information website.

Elsevier hereby grants permission to make all its COVID-19-related research that is available on the COVID-19 resource centre - including this research content - immediately available in PubMed Central and other publicly funded repositories, such as the WHO COVID database with rights for unrestricted research re-use and analyses in any form or by any means with acknowledgement of the original source. These permissions are granted for free by Elsevier for as long as the COVID-19 resource centre remains active.

Infection, Genetics and Evolution 103 (2022) 105318

Contents lists available at ScienceDirect

Infection, Genetics and Evolution

journal homepage: www.elsevier.com/locate/meegid

Research paper

In silico drug repurposing against SARS-CoV-2 using an integrative transcriptomic profiling approach: Hydrocortisone and Benzhydrocodone as potential drug candidates against COVID-19

SeyedehMozhdeh Mirmohammadi [a,b,1], Anvarsadat Kianmehr [a,b,*,1], Amir Sabbaghian [c], Alireza Mohebbi [d], Hamid Shahbazmohammadi [e], Mehdi Sheykharabi [f], Zahra Bazzi [b]

[a] Infectious Diseases Research Center, Golestan University of Medical Sciences, Gorgan, Iran
[b] Department of Medical Biotechnology, School of Advanced Technologies in Medicine, Golestan University of Medical Sciences, Gorgan, Iran
[c] Department of Molecular Medicine, School of Advanced Technologies in Medicine, Golestan University of Medical Sciences, Gorgan, Iran
[d] Vista Aria Rena Gene Inc., 4913817644 Gorgan, Iran
[e] Enzyme Technology Laboratory, Department of Biochemistry, Genetic and Metabolism Research Group, Pasteur Institute of Iran, Tehran, Iran
[f] Department of Medical Nanotechnology, School of Advanced technologies in Medicine, Golestan University of Medical Sciences, Gorgan, Iran.

ARTICLE INFO

Keywords:
COVID-19
SARS-CoV-2
Transcriptomics
Drug repurposing
In silico

ABSTRACT

COVID-19 pathogenesis is mainly attributed to dysregulated antiviral immune response, the prominent hallmark of COVID-19. As no established drugs are available against SARS-CoV-2 and developing new ones would be a big challenge, repurposing of existing drugs holds promise against COVID-19. Here, we used a signature-based strategy to delve into cellular responses to SARS-CoV-2 infection in order to identify potential host contributors in COVID-19 pathogenesis and to find repurposable drugs using in silico approaches. We scrutinized transcriptomic profile of various human alveolar cell sources infected with SARS-CoV-2 to determine up-regulated genes specific to COVID-19. Enrichment analysis revealed that the up-regulated genes were involved mainly in viral infectious disease, immune system, and signal transduction pathways. Analysis of protein-protein interaction network and COVID-19 molecular pathway resulted in identifying several anti-viral proteins as well as 11 host pro-viral proteins, ADAR, HBEGF, MMP9, USP18, JUN, FOS, IRF2, ICAM1, IFI35, CASP1, and STAT3. Finally, molecular docking of up-regulated proteins and all FDA-approved drugs revealed that both Hydrocortisone and Benzhydrocodone possess high binding affinity for all pro-viral proteins. The suggested repurposed drugs should be subject to complementary in vitro and in vivo experiments in order to be evaluated in detail prior to clinical studies in potential management of COVID-19.

1. Introduction

The ongoing outbreak of coronavirus disease 2019 (COVID-19), caused by severe acute respiratory syndrome coronavirus 2 (SARS-CoV-2), pose a massive threat to public health across the globe. SARS-CoV-2 infection was first reported in Wuhan, China, in December 2019 and dubbed a pandemic by the world health organization (WHO) within a short period after the disease outbreak. Together with its highly pathogenic predecessors, SARS and Middle East respiratory syndrome coronavirus (MERS) causing similar infections during last two decades, SARS-CoV-2 belongs to beta-coronaviruses. Beta-coronaviruses possess enveloped, positive-sense single-stranded RNA with 5′-cap structure and 3′-poly-A tail as a typical genomic structure of coronaviruses (CoVs). Indeed, SARS-CoV-2 genome encodes 4 main structural proteins: spike (S), envelope (E), membrane (M), and nucleocapsid (N); it also contains 16 nonstructural proteins (nsp1–16), as well as 7 accessory proteins (ORF3a, ORF3b, ORF6, ORF7a, ORF7b, ORF8, and ORF10) (Mirmohammadi et al., 2020; Ortiz-prado et al., 2020; Ribero et al., 2020). COVID-19 proved to be heterogeneous in its clinical course, as what have made the clinicians puzzled; the majority of SARS-CoV-2 infected patients (nearly 80%) show, if not asymptomatic, a range of mild to moderate symptoms (e.g., cough, fever, etc) which do not require

* Corresponding author at: Department of Medical Biotechnology, School of Advanced technologies in Medicine, Golestan University of Medical Sciences, Gorgan, Iran.
E-mail address: kiabiotpro@yahoo.com (A. Kianmehr).
[1] These authors have equal contribution.

https://doi.org/10.1016/j.meegid.2022.105318
Received 2 November 2021; Received in revised form 8 June 2022; Accepted 13 June 2022
Available online 17 June 2022
1567-1348/© 2022 Published by Elsevier B.V. This is an open access article under the CC BY-NC-ND license (http://creativecommons.org/licenses/by-nc-nd/4.0/).

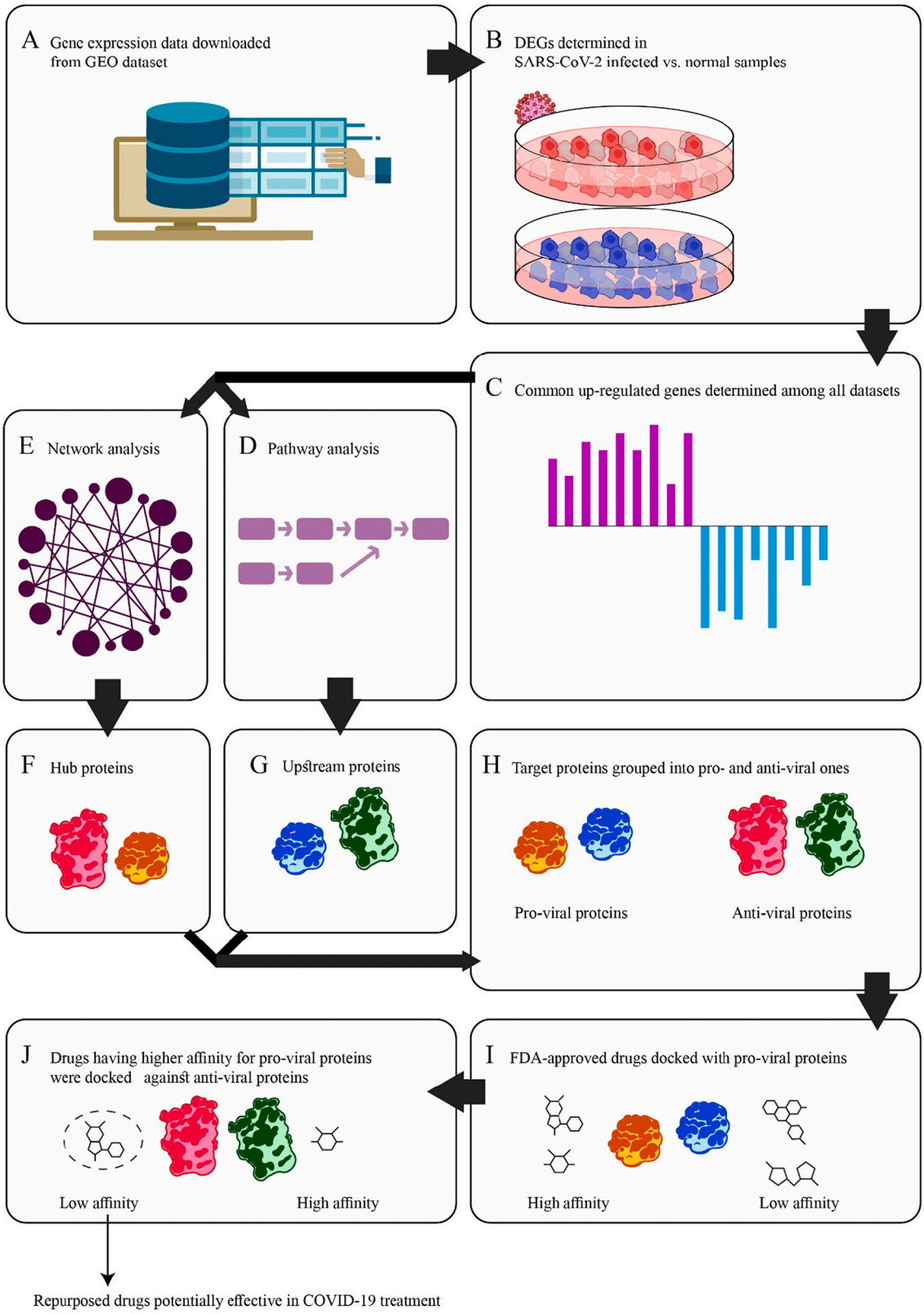

Fig. 1. The overall design of present study.

hospitalization. Of the rest 20%, half of the COVID-19 patients may develop severe pneumonia and acute respiratory distress syndrome (ARDS), and/or multi-organ failure; but, although the underlying mechanism has not been clearly resolved, a mistimed and inadequate antiviral response is supposed to be the reason behind COVID-19 pathogenesis (Lei et al., 2020; Maddah and Modanloo, 2020; Mckechnie and Blish, 2020; Mokhtari et al., 2020). Notably, SARS-CoV-2 infection may contribute to unbalanced immune response, characterized by low levels of type I and III interferons (IFN) expression together with a superfluous pro-inflammatory cytokine response; the latter, so-called as

Table 1
The characteristics of RNA-Seq datasets on various SARS-CoV-2 infected samples.

GEO accession number	Sample type	Sample size	Infected samples	Control	Description
GSE147507	A549 cell line	24	12	12	Independent biological triplicates of transformed lung alveolar (A549) cells were mock treated or infected with SARS-CoV-2 (USA-WA1/2020).
GSE147507	Calu3 cell line	6	3	3	transformed lung-derived Calu-3 cells with a vector expressing human ACE2, were mock treated or infected with SARS-CoV-2 (USA-WA1/2020).
GSE147507	Lung biopsy	16	8	8	Uninfected human lung biopsies were derived from one male (age 72) and one female (age 60) and used as biological replicates. Additionally, lung samples derived from a single male COVID19 deceased patient (age 74) were processed in technical replicates.
GSE147507	Normal Human Bronchial Epithelial Cells (NHBE)	24	12	12	Independent biological triplicates of primary human lung epithelium (NHBE) were mock treated or infected with SARS-CoV-2 (USA-WA1/2020).
GSE153970	Primary human airway epithelial cultures	12	6	6	Primary human airway epithelial cultures were either mock infected (PBS) or infected with SARS-CoV-2.

cytokine storm, accompanied by impaired adaptive host responses has been blamed for extensive local and systemic tissue damages in severe cases of COVID-19 (Balajelini et al., 2020; Blanco-Melo et al., 2020; Catanzaro et al., 2020; Zhou et al., 2020). In essence, the key element in its success for infecting the host cell, as it's true for many respiratory viruses, is either suppressing or evading innate immune response, or using an elaborate integrated strategy to dampen host defenses. As such, SARS-CoV-2 makes best use of host factors for its proliferation and subsequent pathogenesis through driving changes in host gene expression leading to delayed IFN response, which initially plays a vital role in early innate immune response against viruses. Thus, dissecting gene expression profiles of cells infected with SARS-CoV-2, unveiling the perturbations of their transcriptome, may provide valuable insights into dynamics of host immune response as well as critical host contributors (Loganathan et al., 2020). Accordingly, developing effective therapeutic strategies against SARS-CoV-2 requires understanding and analyzing the host transcriptomic data following its infection. On the other hand, drug repurposing provides a unique opportunity to identify new therapies for diseases in a shorter time while it's feasible at lower costs compared with de novo drug development.

Here, we applied an integrative in silico approach basically using transcriptomic RNA-Seq data of COVID-19 to detect differentially expressed genes to elucidate the dynamic transcriptional changes that could underlie the process. We carried out gene-ontology based pathway analysis followed by protein-protein interaction (PPI) network analysis that uncovered upstream proteins and hub proteins as potential targets, respectively. Ultimately, we conducted molecular docking analysis of candidate proteins through the thesaurus of FDA approved drugs to find repurposed drugs interacting with host target proteins with high affinity.

2. Methods and materials

Based on our hypotheses, we conducted pathway and network analysis on genetic profile of SARS-CoV-2 infected cells in order to find the critical up-regulated genes potentially involving in pathogenesis of COVID-19. In next step, all FDA-approved drugs were docked with our list of proteins selected in terms of their contribution to viral pathogenesis. Fig. 1 shows the workflow briefly. In following sections, we will illustrate these steps in detail.

2.1. Extracting expression profile datasets

Gene expression datasets for SARS-CoV-2 infected samples, GSE147507 (9) and GSE153970 (Vanderheiden et al., 2020), were obtained from Gene Expression Omnibus (GEO; www.ncbi.nlm.nih.gov/geo), a freely available public repository of high-throughput datasets (Barrett et al., 2013).

2.2. Identification of differentially expressed genes (DEGs)

We analyzed each RNA-seq dataset separately by using Galaxy platform (https://usegalaxy.eu). First, FastQC 0.11.6 was used to evaluate the sequence reads quality. Then, the Trim Galore (version 0.4.3.1) was employed for adaptor detection and reads were aligned to the reference genome (GRCh38) using HISAT2 (version 2.1.0). The differential expression of genes was calculated using DESeq2 (version 2.11.40.6) followed by selecting genes with log2 fold change>1 and adjusted P-value<0.05 as up-regulated ones. Ultimately, the genetic signature of disease was obtained by recognizing the common up-regulated genes in all datasets.

2.3. Gene ontology and pathway enrichment analysis

Gene set enrichment analysis (GSEA) was done to detect the functional annotation of common significantly up-regulated genes, using Enrichr (https://maayanlab.cloud/Enrichr/), a web based tool visualizing the functional analysis of gene sets (Chen et al., 2013; Kuleshov et al., 2016). Mined data from Kyoto Encyclopedia of Genes and Genome (KEGG) and Gene Ontology (GO) were applied to clarify the potential contribution of up-regulated genes in COVID-19 pathogenesis. Then, significant pathways and GO terms containing those up-regulated genes

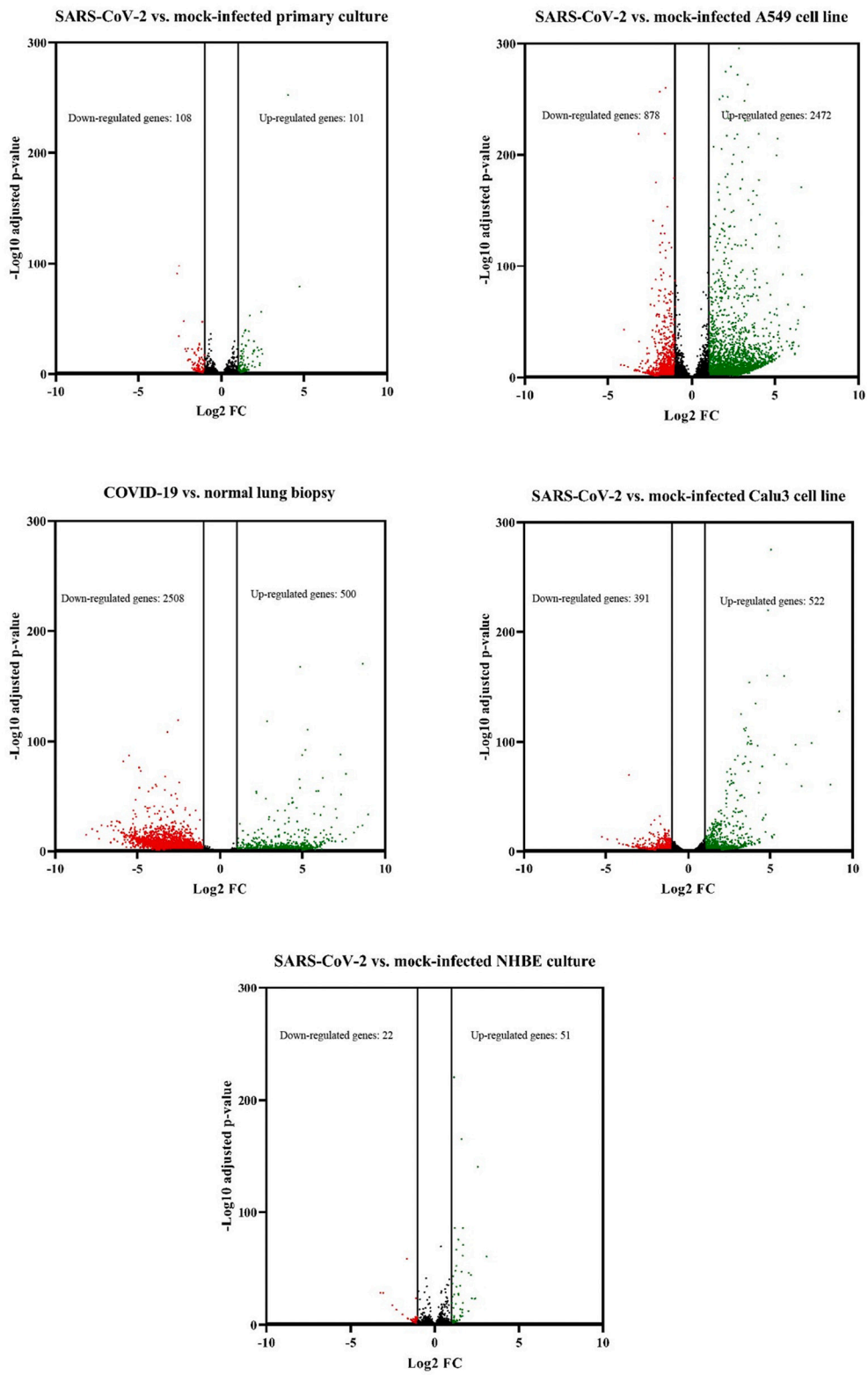

Fig. 2. Volcano plot of DEGs. DEGs were selected applying adjusted p-value<0.05 and Log2 FC > 1 for upregulated and Log2 FC < −1 for down-regulated genes. Finally, 2472, 522, 500, 51, and 101 differentially expressed protein coding genes were selected in A549, Calu3, lung biopsy, NHBE, as well as primary human airway epithelial culture, respectively. In each plot, green dots represent significantly up-regulated genes with expression levels of at least twice in SARS-CoV-2 infected cells compared to that of control group. Also, down-regulated genes, expressed ≤ half in SARS-CoV-2 infected cells in comparison to control, are depicted by red dots. (For interpretation of the references to color in this figure legend, the reader is referred to the web version of this article.)

were selected applying adjusted *P*-value<0.05.

2.4. Protein-protein interactions (PPIs) network analysis

In order to conduct a PPI network and find the hub genes, significantly up-regulated genes were analyzed using STRING (version 11.0; https://string-db.org/), an online protein association network web resource (Szklarczyk et al., 2019). Text mining, experiments, databases, co-expression and co-occurrence were all used as interaction sources and confidence score ≥ 0.9 as minimum required interaction score. Results were then analyzed and visualized using Cytoscape (version 3.7.2) by applying degree, betweenness centrality, and combined score to the node fill color, node diameter, and edge thickness, respectively (Shannon et al., 2003). Nodes possessing high betweenness centrality and

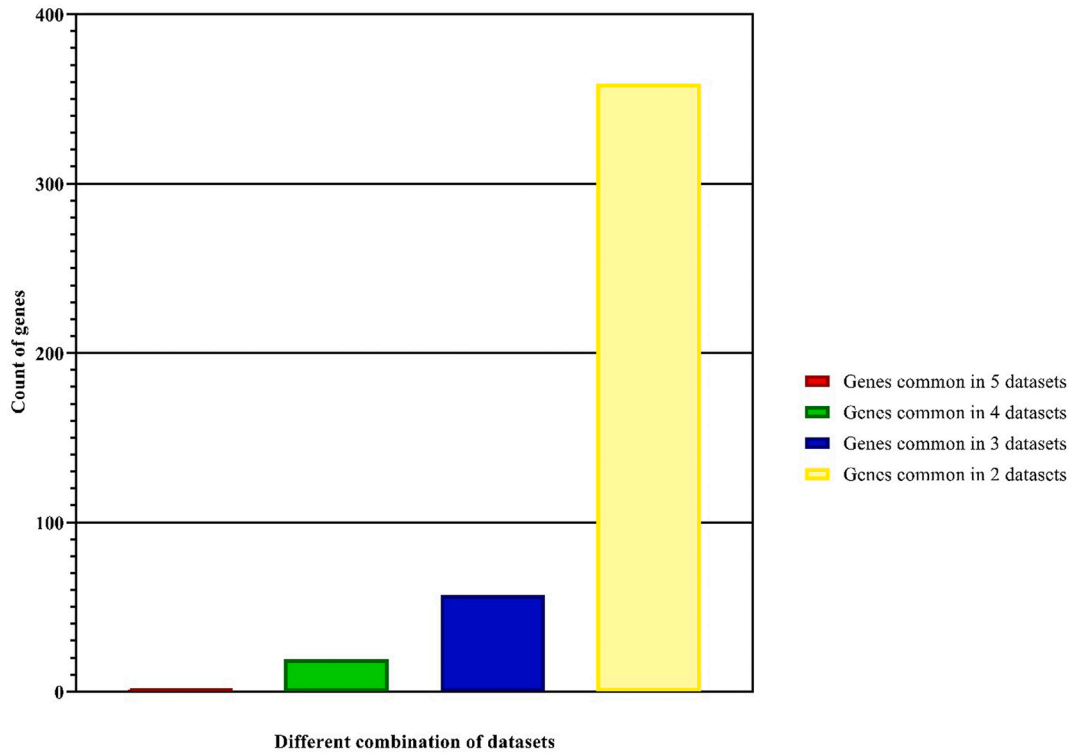

Fig. 3. Bar graph of common up-regulated genes**.** Graph represents the count of common genes among different combination of datasets. Collectively, there are 359 genes common between two datasets (yellow bar), 57 genes among three datasets (blue bar), 19 genes among four datasets (green bar), and only one gene which is common among all 5 datasets (red bar). There are also 2676 genes that are up-regulated in one dataset (not shown). Overall, there are 436 genes up-regulated at least in 2 datasets which termed as "common up-regulated genes" used for further analysis. (For interpretation of the references to color in this figure legend, the reader is referred to the web version of this article.)

Table 2
Common up-regulated genes among 4 and 5 datasets. This table demonstrates the 20 common genes which are significantly up-regulated in at least 4 datasets. Genes are sorted by the mean of Log2 FC with descending order. The third column shows the count of datasets in which each gene is significantly up-regulated.

Gene	Log2 FC (mean)	Count of datasets
SAA2	2.249372	5
OAS2	3.733138	4
CSF2	3.711084	4
RSAD2	3.506331	4
CXCL10	3.477738	4
IFI44L	3.403838	4
XAF1	3.390731	4
CXCL11	3.339592	4
CXCL8	2.813778	4
OAS1	2.799663	4
CXCL2	2.720947	4
INHBA	2.678362	4
OAS3	2.664406	4
KYNU	2.36684	4
HELZ2	2.286049	4
TNFSF14	1.76611	4
LIF	1.710306	4
HBEGF	1.564305	4
CXCL1	1.550704	4
S100A9	1.540737	4

degree were selected as hub genes. Genes with the degree of equal or >10 and betweenness centrality of equal or >0.001 were chosen as hub genes.

2.5. Pathway analysis

Pathway analysis was conducted in order to find upstream proteins of pathway whose inhibition might lead to disturbed function of downstream proteins. For this purpose, up-regulated genes were mapped in COVID-19 pathway using "Search & Color Pathway" from KEGG mapping online tools (https://www.genome.jp/kegg/mapper/) (Kanehisa and Sato, 2020).

2.6. Evaluating upstream proteins and hub genes

Since the pathological nature of COVID-19 has not been fully understood, previously investigated upstream proteins and hub genes were evaluated based on the evidence indicating their contribution to either COVID-19 or any other viral diseases.

2.7. Preparation of candidate proteins' structure and FDA approved drugs

The sequences of candidate proteins were obtained from UniProt (www.uniprot.org) and prediction of 3D structures from amino acid sequence was done using RaptorX (http://raptorx.uchicago.edu/) web server (Källberg et al., 2012). Also, the structures of all FDA approved drugs were extracted from DrugBank (https://go.drugbank.com/).

2.8. Docking software and parameters

Accordingly, the open-source tool Autodock Vina (Trott and Olson, 2010) was applied in the setting of PaDEL-ADV (www.yapcwsof t.com/dd/padeladv/). Vina is a quick and precise tool for ligand-receptor docking accompanied with PaDEL-ADV that allows high-throughput screenings of several ligands in one run. Then, target proteins were treated as receptor in the MGLTools 1.5.6 software

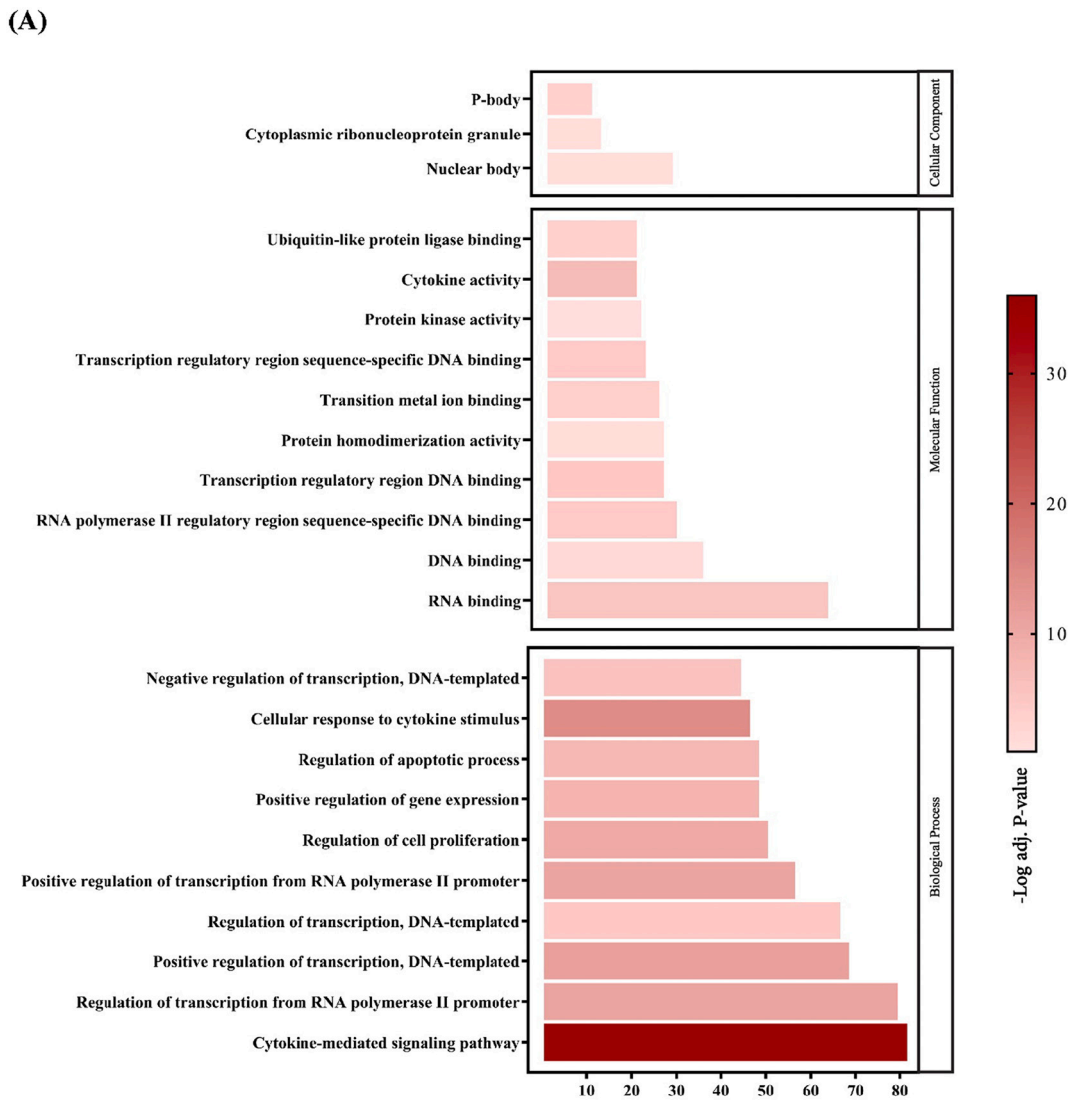

Fig. 4. Gene set enrichment analysis:
(A) Gene ontology enrichment of common up-regulated genes. The graphs represent top 10 significantly (adjusted *p*-value <0.05) enriched biological process and molecular function as well as all significantly enriched cellular component terms, with darker red indicating greater significance. Count of genes are shown in x-axis, while the y-axis represents the GO terms.
(B) KEGG pathway enrichment of common up-regulated genes. Significantly enriched viral infection pathways are indicated here with darker blue standing for greater significance; x-axis shows count of genes involving in each over-presented pathway and y-axis represents the KEGG terms.

(Molecular Graphics Laboratory, The Scripps Research Institute). As such, a grid-box was defined in 3D dimension to include the entire protein. The number of grid points and the spacing were kept to default values. Docking results for each protein were ranked by binding affinity and the affinity of less than −12 kcal/mol was considered high.

3. Results

3.1. Differential gene identification

The detailed characteristics of SARS-CoV-2 infected samples have been presented in Table 1. We analyzed the transcriptomics of each SARS-CoV-2 infected dataset using Galaxy platform. The integrative analysis by DESeq2 revealed 2472, 522, 500, 51, and 101 differentially expressed protein coding genes in A549, Calu3, lung biopsy, NHBE, as well as primary human airway epithelial culture, respectively (Fig. 2). For enriching our list of common genes possibly involving in COVID-19 pathogenesis, we incorporated up-regulated genes which at least exist in two datasets (Fig. 3). DEGs commonly expressed in at least 4 datasets are brought in Table 2 and all common DEGs are presented in Supplementary Table S1 in detail.

3.2. Functional enrichment analysis

To further explore the functional characteristics of common up-regulated genes, we carried out a GO and KEGG pathway enrichment using Enrichr online tool. Considering adjusted *P*-value<0.05, as significance threshold, we identified a total of 46 pathways which are significantly enriched in these 436 up-regulated genes. Significant over-presented pathways largely fell into 3 distinct groups: (1) viral infectious disease such as molecular responses to Influenza A, Herpes simplex virus 1 and Kaposi sarcoma-associated herpesvirus infection (Fig. 4B) (2) immune system and disease such as pathways like NOD-like receptor signaling pathway, IL-17 signaling pathway, and Rheumatoid arthritis, and (3) signal transduction pathways such as TNF signaling pathway, MAPK signaling pathway, and JAK-STAT signaling pathway. Table S2

(B)

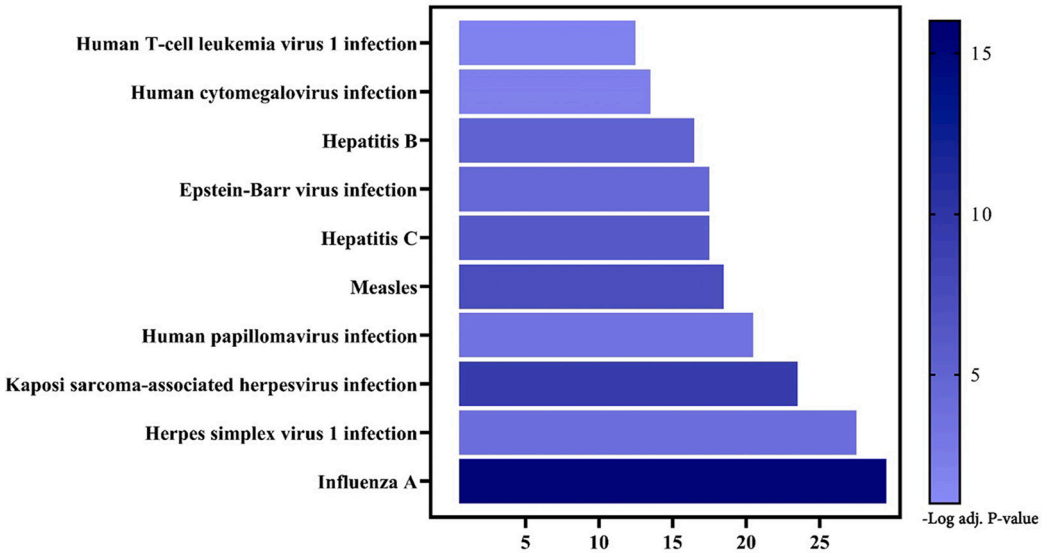

Fig. 4. (*continued*).

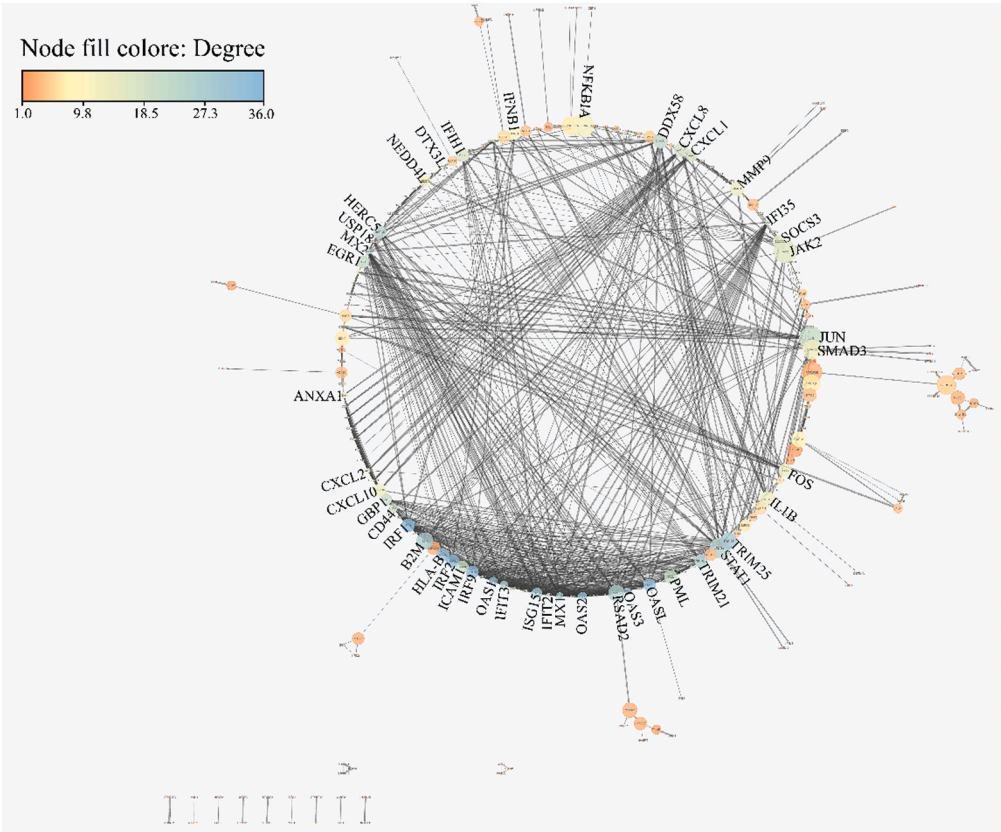

Fig. 5. PPI network analysis of common up-regulated genes. Nodes represent the proteins and edges represent the protein-protein association based on text mining, experiments, databases, co-expression and co-occurrence. The degree, betweenness centrality and combined score are applied to the node fill color, node diameter and edge thickness, respectively. The larger the node diameter, the more the degree; the larger the edge thickness, the more the combined score.

shows the enriched pathways and genes in detail. Results of GO analysis indicated that upregulated genes were expressively enriched in biological processes (BP), such as cytokine-mediated signaling pathway, regulation of transcription from RNA polymerase II promoter, and positive regulation of transcription; in molecular function (MF), such as RNA binding and DNA binding; and in significant cell component (CC),

Table 3
Hub genes. Top proteins are presented based on topological properties in PPI network of common up-regulated genes, and listed in terms of decreasing degree of betweenness centrality.

Hub gene	Betweenness centrality	Degree
IRF1	0.034676	36
IRF9	0.027837	35
IRF2	0.025367	35
OASL	0.024146	34
HLA-B	0.024814	33
OAS1	0.009873	33
OAS2	0.009747	33
OAS3	0.007155	32
TRIM25	0.073805	29
ISG15	0.012916	29
B2M	0.08053	28
IFIT3	0.009114	27
MX1	0.007065	27
RSAD2	0.06993	26
TRIM21	0.029485	26
STAT1	0.125145	25
HERC5	0.032096	25
MX2	0.005832	25
IFIT2	0.002126	23
DDX58	0.051766	22
EGR1	0.0203	22
JUN	0.163334	21
PML	0.035144	21
ICAM1	0.022862	21
GBP1	0.013701	21
CD44	0.010007	20
IFI35	0.004453	20
CXCL8	0.045278	18
CXCL1	0.020933	18
IFIH1	0.032595	17
JAK2	0.152983	16
SOCS3	0.040662	16
MMP9	0.045439	14
IL1B	0.066334	13
FOS	0.035632	13
CXCL10	0.029658	13
ANXA1	0.006606	13
NFKBIA	0.161759	12
SMAD3	0.11005	12
CXCL2	0.003424	12
NEDD4L	0.016034	11
DTX3L	0.002662	11
IFNB1	0.017094	10
USP18	0.001043	10

such as nuclear body and cytoplasmic ribonucleoprotein granule (Fig. 4A). Table S3 represents the enriched ontologies and genes in detail.

3.3. PPI Network analysis

All up-regulated protein-coding genes were imported to the STRING database. Afterwards, the confidence score of >0.9 was set as cutoff criterion and host protein interactome of 355 nodes and 831 edges was constructed and underwent analysis by using Cytoscape to illustrate their intricate relationships (Fig. 5). Here we chose genes having high betweenness centrality and degree as hub genes (Table 3).

3.4. Pathway analysis

In order to find upstream proteins, which their inhibition may affect down-stream molecular processes, all common up-regulated genes were spotted in COVID-19 pathway (Fig. 6). Upstream proteins are presented in Table 4.

3.5. Target protein classification

Based on supporting evidence for contribution of hub genes and upstream proteins in COVID-19 and other viral infections, we categorized them into pro- and anti-viral genes (Table 5). Fig. 7 shows the expression level of genes coding target proteins in each dataset.

3.6. Assessment of FDA approved drugs interactions with candidate genes

As shown in Table 6, out of 2470 FDA-approved drugs 68 compounds have high affinity for all of the pro-viral proteins. These 68 compounds were then docked against anti-viral proteins to find the drugs that have low interaction energy for almost all of anti-viral proteins. The results indicated that Hydrocortisone and Benzhydrocodone interacted strongly with all pro-viral proteins; also, they demonstrated low affinity for more than half of anti-viral proteins. These two compounds could be introduced as potentially effective blockers with probable negative influence on ADAR, HBEGF, MMP9, USP18, JUN, FOS, IRF2, ICAM1, IFI35, CASP1, and STAT3 with therapeutic benefits. Table 7 represents the characteristics of these two drugs in details.

4. Discussion

To date, therapeutic approaches toward SARS-CoV-2 infection mainly encompass either antiviral agents or immunomodulatory therapy (Ortiz-prado et al., 2020). Several lines of research suggest the host inflammatory response as the main source of clinical symptoms and, at the same time, as a promising therapeutic target. Although, our knowledge concerning host defense against SARS-CoV-2 is mounting, there still seems a lot to explore when it comes to seeking a robust remedy (Mckechnie and Blish, 2020; Shi et al., 2020; Tufan et al., 2020). Typically, significant changes in host transcriptome following viral infection could result in abnormal metabolism of host cells, which in turn set the stage for viral multiplication and its subsequent pathogenesis (Blanco-Melo et al., 2020). Here, an exhaustive human-SARS-CoV-2 interactome was established using RNA-Seq transcriptomes of the lung epithelial cells infected with SARS-CoV-2 versus mock infected cells. In line with previous findings, our initial GO analysis based on DEGs depicted significant enrichment of biological processes mainly pivoting around innate immune response to viral infections and inflammatory pathways, including cytokine-cytokine receptor interaction, TNF signaling, interferon signaling, IL-17 signaling, NF-kB signaling, and chemokine signaling (Blanco-Melo et al., 2020; Zhou et al., 2020). As expected, pathway enrichment was predominated by viral diseases, namely, Influenza A, Measels, Hepatitis B and C, Epstein-Barr virus infection, Human papillomavirus infection, and so on. These pathways clearly underline immune system's involvement in host response to SARS-CoV-2 infection via early innate immune response, pointing to a huge avenue which provides unique drug repurposing opportunities in COVID-19. Recent findings suggest that SARS-CoV-2 infection defies the prevailing paradigm of antiviral immunity, in which IFN-mediated antiviral defenses normally precede the pro-inflammatory response; in other words, SARS-CoV-2 infection triggers pro-inflammatory cascade far earlier than IFN-mediated antiviral responses; indeed, initial IFN response found to be stronger in patients with mild to moderate COVID-19 than the ones in critical condition (Galani et al., 2021). This unusual order observed during SARS-CoV-2 infection, unlike influenza virus, helps explain some of its unique properties observed in COVID-19 (e.g., delayed or reduced IFN production may account for longer viral incubation period in upper respiratory tract). Not surprisingly, SARS-CoV-2 has evolved strategies mainly focused on inhibiting type I/III IFN production pathway, i.e. several SARS-CoV-2 proteins antagonize IFN production via distinct mechanisms. In particular, we found up-regulated genes largely among interferon-stimulated genes (ISGs) having different functions directly or indirectly in host's combat against SARS-CoV-2. As the sensors of viral DNA and RNA structures, termed as

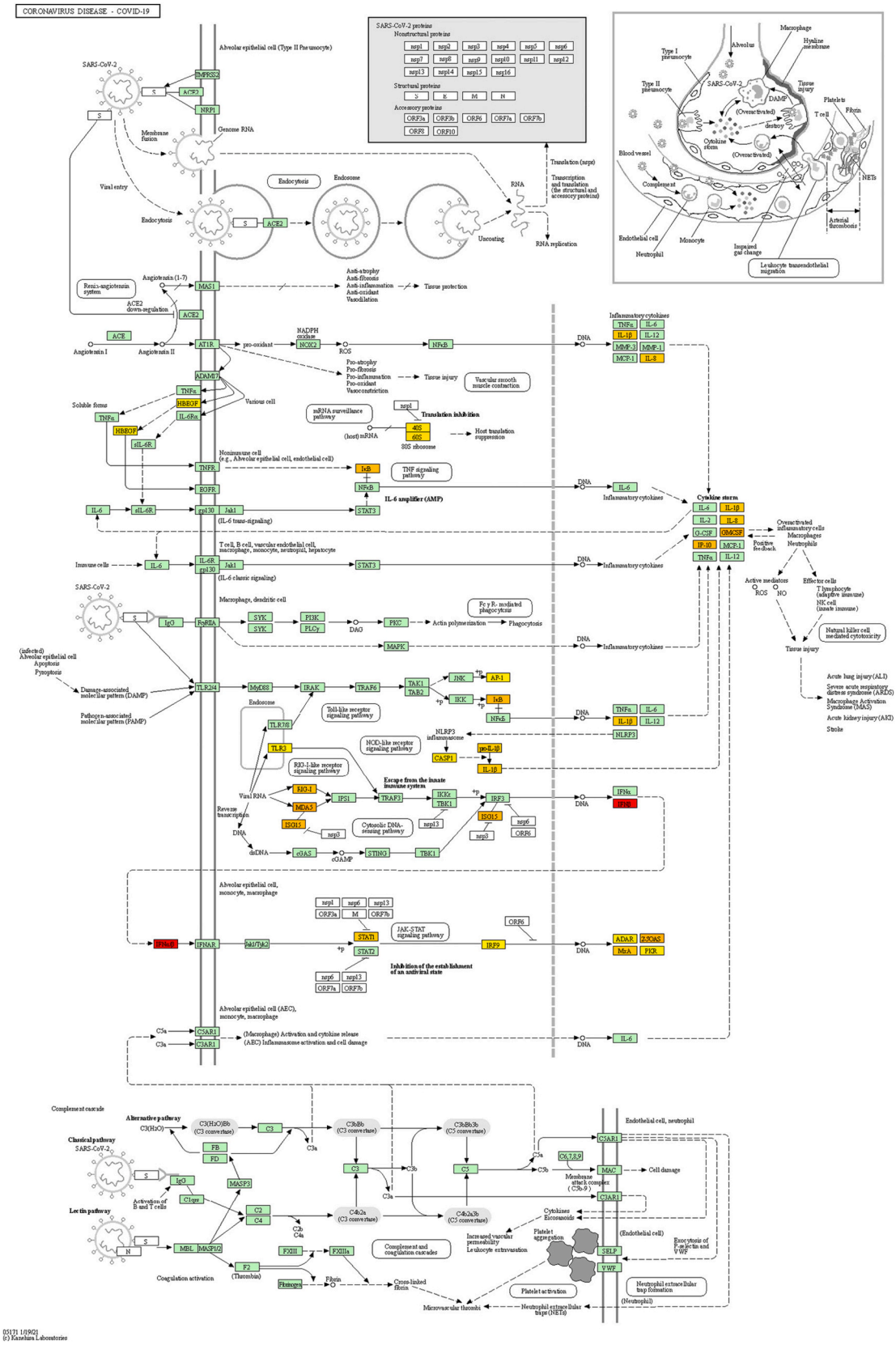

Fig. 6. Pathway of COVID-19 represented in KEGG. Common up-regulated genes were located in the proposed pathway of COVID-19 using KEGG mapper online tool. Colored genes are shown to be significantly up-regulated in our study and intensity of color shows the Log2 FC. Red shows the highest and yellow shows the lowest Log2 FC. (For interpretation of the references to color in this figure legend, the reader is referred to the web version of this article.)

Table 4
Pathway analysis results. It shows upstream proteins and corresponding downstream proteins which could be affected. For inhibition, upstream proteins only are targeted, except the ones that activate both anti- and pro-viral proteins (e.g. IFN α/β activation leads to activation of various anti-viral (STAT1, IRF9, OAS1, OAS2, OAS3, MX1, EIF2AK2) and pro-viral proteins (ADAR). In this case, only ADAR is a target of inhibition.)

Upstream protein	Downstream protein/proteins
HBEGF	EGFR
NFKBIA (IκB)	IL1β, IL8, CSF2 (GMCSF), CXCL10 (IP10)
STAT3	IL1β, IL8, CSF2 (GMCSF), CXCL10 (IP10)
TLR3	IFNβ
CASP1	IL1β, IL8, CSF2 (GMCSF), CXCL10 (IP10)
IFNα, β	STAT1, IRF9, ADAR, OAS1, OAS2, OAS3, MX1 (MXA), EIF2AK2 (PKR)
ISG15	IFNβ
IFIH1 (MDA5)	IFNβ
DDX58 (RIGI)	IFNβ

pattern-recognition receptors (PRRs), DDX58 (RIG-I), IFIH1 (MDA5), EIF2AK2 (PKR), and TLR3 all are among ISGs found to be activated in SARS-CoV-2-infected samples. However, each one recognizes a distinct viral nucleic acid structure, inducing separate intracellular signaling pathways. Influenza A virus (IAV) infection has been shown to trigger both TRL3, a dsRNA sensor, leading to a pro-inflammatory response, and DDX-58/RIG-I, sensing ssRNA with free 5′-triphosphate end, activating type I IFN-mediated antiviral signaling as well as pro-inflammatory response (Le Goffic et al., 2007). Of note, DDX-58/RIG-I and IFIH1/MDA5 both trigger their signaling pathways via common adaptor mitochondrial antiviral signaling protein (MAVS), located on mitochondrial outer membrane, to induce a series of antiviral genes including type I IFN (Mirmohammadi et al., 2020). Further, the IFN-regulatory factor (IRF) family proteins, as transcription factors, function to bridge the sensing of microbial signatures to the expression of IFNs and pro-inflammatory cytokines (Samuel, 2001). The resulting IFNs, including IFN-α, IFN-β, IFN-γ, trigger ISG expression to promote antiviral responses through the activation of IFN receptor associated Janus kinase-signal transducer and activator of transcription (JAK-STAT) pathway (Lee and Shin, 2020; Park and Iwasaki, 2020). In our analysis, we found 3 up-regulated IRFs as our hub genes among which IRF-1 plays a prominent role in stimulating IFN gene expression during viral infection; in contrast, IRF-2 inhibits it; and IRF-9 together with JAK2 and STAT1 belong to a subset of ISGs that enhance JAK-STAT signaling to establish an antiviral state (Samuel, 2001). Induction of antiviral ISGs, such as radical S-adenosyl methionine domain containing 2 (RSAD2)/viperin, MX Dynamin Like GTPase (MX1), MX2, ISG15 in addition to OAS1–3 were commonly reported in a wide range of viral infections including COVID-19 (Bizzotto et al., 2020; Kurokawa et al., 2019; Lindner et al., 2007; Swaim et al., 2020; Verhelst et al., 2012).

4.1. Potential host proteins as candidates for inhibition

In addition to up-regulated antiviral genes, expression of some pro-viral genes involving in virus-mediated infection was found to be increased as well. We based our interpretation on previous studies on other viruses that may point to these proteins as likely contributors in SARS-CoV-2 infection and as potential targets for drug repurposing, including ADAR, HBEGF, MMP9, USP18, JUN, FOS, IRF2, ICAM1, IFI35, CASP1, and STAT3.

In an earlier study on SARS-CoV-induced lung fibrosis using mice models, authors found that amphiregulin (AREG) and heparin-binding EGF-like growth factor (HB-EGF) were among up-regulated genes in SARS-CoV infected mice. They further indicated that persistent activation of EGFR via AREG and HB-EGF caused lung tissue fibrosis (Venkataraman et al., 2017). Activation of EGFR signaling may have a range of outcomes, such as the inhibition of apoptosis, increased proliferation

Table 5
Literature review results. This table shows the results of literature review on hub proteins of network and upstream protein of COVID-19 pathway in terms of their contribution to viral infection. Based on our hypothesis, the proposed drug must be capable of inhibiting pro-viral or inflammatory proteins and not the anti-viral ones.

Protein	Function	Reference
Proteins not to be inhibited		
IRF1	A transcription factor for inducing IFNs expression	[29]
IRF9	A transcription factor for inducing IFNs expression	[29]
STAT1	A transcription factor forming dimer with STAT2 to induce ISGs expression	[29]
OASL	Mediates DDX-58/RIG-I activation	[35]
OAS1	Induction of RNA degradation by activating RNaseL	[36]
OAS2	Induction of RNA degradation by activating RNaseL	[36]
OAS3	Induction of RNA degradation by activating RNaseL	[36]
MX1	Interrupts viral ribonucleoprotein complex formation	[40]
MX2	It interrupts viral ribonucleoprotein complex formation	[42]
RSAD2	Localized on ER, it's an ISG playing role in inhibiting various DNA and RNA viruses	[41]
TRIM21	An E3 ubiquitin ligase interacting with MAVS to positively regulate innate immunity	[61]
TRIM25	An E3 ubiquitin ligase in RIG-I signaling pathway	[61]
ISG15	A Ubiquitin-like protein playing a key role in the innate immune response to viral infection via its conjugation to a target protein (ISGylation)	[43]
PML	Functions via its association with PML-nuclear bodies (PML-NBs)	[61]
IFIT2	Inhibition of viral replication	[44]
IFIT3	Inhibition of viral replication	[46]
DDX58	An innate immune receptor acting as a cytoplasmic sensor of viral nucleic acids	[28]
HERC5	An E3 ligase required for the conjugation of ISG15 to target proteins	[61]
GBP1	Promotes oxidative killing and delivers antimicrobial peptides to autophagolysosomes	[61]
EIF2AK2	A protein kinase that phosphorylates the alpha subunit of eukaryotic translation initiation factor 2 (EIF2S1/eIF-2-alpha) and plays a key role in the innate immune response to viral infection	[61]
DTX3L	E3 ubiquitin-protein ligase playing a role in DNA damage repair and in interferon-mediated antiviral responses	[61]
IFNB1	Encodes a cytokine belonging to the interferon family of signaling proteins, released as part of the innate immune response to pathogens	[32]
NEDD4L	An E3 ubiquitin ligase which regulates epithelial and voltage-gated sodium channels	[61]
TLR3	A nucleotide-sensing TLR which is activated by double-stranded RNA	[26]
CSF2	Controls the production, differentiation, and function of granulocytes and macrophages	[61]
CD44	A cell-surface adhesion molecule and hyaluronan receptor	[61]
IFIH1	Acts as a cytoplasmic sensor of viral nucleic acids	[27]
SMAD3	Functions in the transforming growth factor-beta signaling pathway, and transmits signals from the cell surface to the nucleus	[61]
ANXA1	Plays important roles in the innate immune response as effector of glucocorticoid-mediated responses and regulator of the inflammatory process	[61]
NFKBIA	Inhibits NF-kappa-B complexes which are involved in inflammatory responses	[61]
SOCS3	Involves in negative regulation of cytokines that signal through the JAK/STAT pathway	[29]
Proteins to be inhibited		
ADAR	Catalyzes the conversion of adenosine (A) to inosine (I) in double-stranded RNA (dsRNA) substrates	[56]
HBEGF	A mitogenic growth factor playing role in wound healing	[48]
MMP9	Degrades a broad spectrum of extracellular matrix (ECM) proteins and plays a role in acute lung injury	[53]
USP18	Involves in the regulation of inflammatory response to interferon type 1	[60]
STAT3	In response to cytokines and growth factors, it translocates to the cell nucleus where acts as transcription activator	[61]
JUN	Transcription factor that recognizes and binds to the enhancer heptamer motif 5′-TGA[*CG*]TCA-3’	[61]

(*continued on next page*)

Table 5 (*continued*)

Protein	Function	Reference
FOS	Nuclear phosphoprotein which forms a tight but non-covalently linked complex with the JUN/AP-1 transcription factor	[61]
IRF2	A transcription factor playing role in suppressing IFNs	[29]
ICAM1	Ligand for the leukocyte adhesion protein LFA-1	[57]
IFI35	Negative regulation of RIG-I-mediated antiviral signaling	[61]
CASP1	Initiates a proinflammatory response through the cleavage of the two inflammatory cytokines IL1B and IL18	[61]

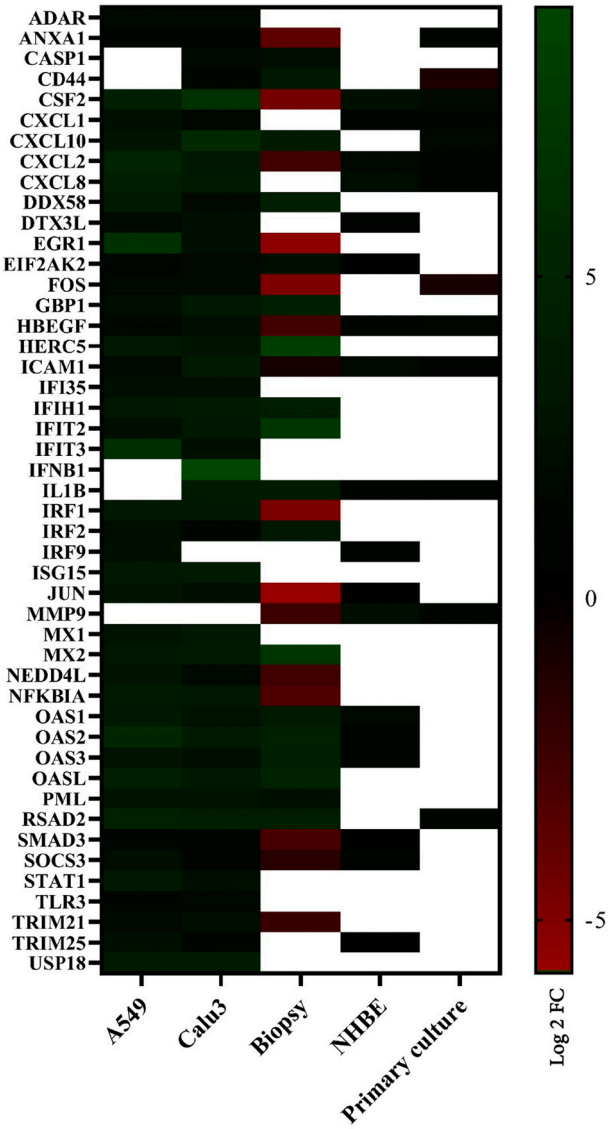

Fig. 7. Heatmap of differential expression of critical genes in each dataset. It summarizes expression data for … genes considered as contributors of COVID-19 pathogenesis. Color intensity represents log 2 fold change. Red and green colors show down-, and up-regulation of genes in SARS-CoV-2 infected samples vs. control in each dataset. While white means that the gene has no significant change in expression level during viral infection. (For interpretation of the references to color in this figure legend, the reader is referred to the web version of this article.)

and migration, activation of the inflammatory response and increase in mucus production (Venkataraman and Frieman, 2017). In line with a recent work (Hazra et al., 2020), our results demonstrate that EGFR signaling is a key regulator of SARS-CoV-induced lung damage and that targeting this response could protect against the development of pulmonary fibrosis caused by respiratory viruses such as SARS-CoV. Matrix metalloproteinase 9 (MMP9), also known as gelatinase B; type IV collagenase, is expressed by epithelial cells, endothelial cells, and all leukocytes. It regulates acute lung injury, disrupts airway epithelial barrier function, and degrades a broad spectrum of extracellular matrix (ECM) proteins as well (Yoshizaki et al., 1998). Two separate studies on influenza virus A (IVA) models concluded that the MMP9 increased expression during IAV infection resulted in enhanced mortality due to acute lung injury and pulmonary inflammation (Rojas-Quintero et al., 2018; Villeret et al., 2020).

Similar works reported improved survival rates in IAV-infected MMP9 knock-out compared to wild type mice; this has been attributed to some factors as likely explanation including lower lung viral burden, enhanced pulmonary adaptive immune response, and less severe lung injury (Herold et al., 2015; Quintero et al., 2010). The adenosine deaminases acting on RNA (ADARs) are double-stranded RNA (dsRNA) binding enzymes that catalyze RNA editing of viral dsRNAs from adenosine to inosine (A-to-I). The ADAR1 gene is expressed in most human tissues; it serves as master regulator of cytoplasmic innate immunity regulating multiple microbial nucleic acid sensors, such as MDA5, RIG-I, OAS and PKR, which detect intracellular dsRNA of viruses including SARS-CoV-2 (Gélinas et al., 2011). Intercellular adhesion molecule 1 (ICAM-1), a member of the immunoglobulin super-gene family, is an adhesive ligand for leukocytes. The endothelial expression of ICAM-1 was significantly higher in the COVID-19 group than H1N1 and control groups. The activated endothelial cells can express the ICAM-1 molecules to transmit intracellular signals causing prolonged pro-inflammatory status. The proinflammatory condition would result in a systemic endothelial dysfunction and lead to the loss of its integrity via endothelial cell death. Thus, persistent inflammatory signaling of these adhesion molecules would also contribute to later thrombotic events (Jin et al., 2020; Nagashima et al., 2020). Importantly, ubiquitin-specific protease 18 (USP18) has the major ISG15 specific protease activity which counteracts ISG15 conjugation, thereby removing ISG15 from ISG15-conjugated proteins (Ritchie et al., 2004). Loss of USP18 in mice led to resistance to the cytopathic effects caused by some viruses including lymphocytic choriomeningitis virus (LCMV), vesicular stomatitis virus (VSV), and Sindbis virus (Kim et al., 2008). The broad array of physiological functions and regulation of ISG15 and USP18 offers a variety of potential intervention strategies which could be of therapeutic use.

COVID-19 drug repurposing was done by docking hub and upstream proteins with FDA-aprroved drugs. As mentioned earlier hub and upstream proteins fell into two groups, pro-virals and anti-virals. Our criteria for selecting a FDA-approved drug potentially effective in controlling COVID-19 were: (1) High binding affinity for all pro-viral proteins and (2) Low binding affinity for all (or at least half of) anti-viral proteins.

Among pro-viral proteins, we selected ADAR, HBEGF, MMP9, USP18, ICAM1, CASP1, STAT3, IRF2, FOS, JUN, and IFI35. EGR1 was eliminated because it was in the down-stream of STAT3 activation. Among 2470 FDA-approved drugs, peptides were eliminated and a list of 2413 small molecules was selected for further analysis. Docking analysis of FDA-approved drugs with these eleven proteins resulted in varied affinities that were filtered (<-12 kcal/mol) and a list of 68 drugs capable of binding to all pro-viral proteins were obtained. In the next step, these drugs were docked with anti-viral proteins and results revealed that two drugs, Hydrocodone and Benzhydrocodone, had low affinity for more than half of anti-viral proteins.

5. Conclusion

Currently, effective COVID-19 management encountered shortcomings in vaccine supply, public compliance, undefined duration of immunity, and potential for mutation of vaccine targets all suggest the

Table 6
Docking results. In this table, the results of docking FDA-approved drug and antiviral proteins with high affinity (less than −12 kcal/mol) are presented. The first column represents the generic name of the drug, and in other columns, antiviral proteins and their affinity for each drug are brought.

Drugs	Docking results of pro-viral proteins										
	ADAR	HBEGF	MMP9	USP18	JUN	FOS	IRF2	ICAM1	IFI35	CASP1	STAT3
Flunisolide	−14.7556	−12.6	−17.0222	−13.82	−13.1222	−12.4625	−12.5556	−16.1667	−12.6167	−13.6	−17.0889
Azithromycin	−12.4556	−12.7429	−14.4667	−12.6333	−12.6143	−13.1889	−13.8556	−14.2778	−13.1667	−12.9444	−18.5778
Diflorasone	−13.2111	−12.2	−15.7	−12.62	−12.225	−12.125	−12.4667	−13.5444	−12.4667	−12.375	−16.9667
Alclometasone	−13.7778	−12.7	−16.6667	−12.6444	−12.7111	−12.6556	−12.6667	−15.7778	−12.4444	−12.7889	−18
Medrysone	−12.6778	−12.3	−15.3667	−12.35	−12	−12.1	−12.35	−14.8667	−12.45	−12.7143	−16.9222
Vindesine	−13.9556	−13.2333	−13.7333	−12.7778	−12.1	−12.6333	−13.7444	−12.7	−13.125	−13.3667	−13.5111
fluorometholone	−14.0111	−12.225	−16.3556	−12.6667	−12.16	−12.35	−12.3556	−14.9333	−12.7333	−12.6125	−17.2778
Betamethasone	−14.0333	−12.45	−15.9111	−12.625	−12.4	−12.3	−12.4	−15.0333	−12.3714	−12.56	−17.3778
Fluocinolone acetonide	−14.7667	−12.6111	−17.0667	−13.74	−12.5667	−12.8	−12.6444	−14.4444	−13.4778	−13.2222	−18.7111
Oxytetracycline	−13.8222	−12.125	−15.6	−13.425	−12.55	−12.2222	−12.5778	−14.7889	−12.4667	−12.4286	−17.5778
Ulobetasol	−14.0667	−12.5	−16.6111	−13.0857	−12.7333	−12.6111	−12.5222	−15.5333	−13.0556	−12.9111	−18.2
Rifabutin	−15.9333	−15.0667	−17.2444	−14.9111	−13.7167	−15.7556	−16.6778	−18.1571	−16.1556	−14.8222	−21.1778
Oxandrolone	−14.9333	−12	−15.4444	−12.6	−12.4	−12.1	−12.4	−13.8111	−12.275	−12.8	−16.2
Nystatin	−16.4333	−15.1444	−18.9778	−14.9111	−15.1889	−16.5778	−17.7	−17.5889	−16.6778	−15.2222	−23.9222
amphotericin B	−16.8	−15.1667	−19.0111	−15.0222	−14.8	−16.6556	−17.7889	−17.5111	−16.4778	−15.1444	−23.0111
Fluorescein	−13.2111	−12.3	−15.7	−12.24	−12.2	−12	−12.575	−15.0778	−12.3	−12.85	−17.1778
Ergotamine	−12.7778	−13.8444	−15.5111	−13.1111	−12.6667	−12.32	−13.6111	−13.9333	−12.3444	−14.5111	−20.575
Eplerenone	−13.5778	−12.8	−15.4778	−12.775	−12.3333	−12.1667	−12.7	−14.9222	−12.4125	−12.5111	−17.0444
Hydrocortisone	−12.8	−12	−15.6556	−12	−12	−12	−12.1667	−14.0667	−12.4	−12.575	−16.3556
Irinotecan	−13.3667	−12.5333	−15.2	−12.2667	−12.1	−12.0667	−13.5333	−16.6	−12.76	−12.4625	−18.3778
Natamycin	−14.6444	−13.4333	−15.3889	−13	−13.0125	−13.7778	−13.9889	−15.2222	−13.3333	−13.2778	−19.8889
Prednisolone	−12.6667	−12.3	−15.6889	−12.425	−12.3	−12.2333	−12.525	−14.5667	−12.75	−12.7143	−16.4333
Rimexolone	−12.9286	−12.36	−16.2556	−12.55	−12.6333	−12	−12.85	−15.3111	−12.525	−12.6111	−17.3778
Metacycline	−13.4556	−12	−15.4444	−12.82	−12.6	−12.5	−12.3857	−14.4222	−12.26	−12.525	−16.8889
Methylprednisolone	−14.0333	−12.525	−16.5333	−12.475	−12.48	−12.4111	−12.25	−14.8889	−12.4167	−13	−17.6444
Rifampicin	−14.1778	−13.3444	−16.0111	−13.4778	−12.25	−12.975	−14.4778	−13.75	−14.4222	−13.6444	−19.25
Candicidin	−14.3222	−13.5111	−17.2444	−12.7	−13.0444	−13.9667	−16.5556	−13.1778	−14.9	−12.8778	−20.5222
Idarubicin	−12.8222	−12.12	−15.5889	−12.8167	−12.16	−12.2429	−12.4444	−15.4222	−12.4167	−12.6143	−18.4889
Fluoxymesterone	−13.6667	−12.3	−16.1111	−12.4	−12.28	−12.3	−12.825	−14.5778	−12.625	−12.8857	−17.1778
Tubocurarine	−17.1333	−13.1556	−17.5667	−13.1889	−13.2667	−14.3222	−14.7889	−16.0556	−14.7333	−13.6222	−20.5111
Rifapentine	−15.9667	−14.2778	−16.8222	−14.0889	−13.2	−14.6556	−15.0778	−17.3222	−15.1889	−14.1222	−20.9333
Rifaximin	−15.6333	−14.2222	−17.4	−14.4889	−12.9778	−15.0778	−15.7778	−17.7556	−14.6333	−14.5889	−21.8333
Budesonide	−13.3667	−12.3	−15.5111	−12.5	−12.1	−12.175	−12.5	−14.7111	−12.4222	−12.26	−17.3222
Dexamethasone	−13.4	−12.4	−16.1667	−12.7857	−12.3429	−12.4167	−12.5333	−15.0556	−12.5286	−12.55	−17.6444
Retapamulin	−14.0444	−12.3333	−16.3111	−12.3444	−12.22	−12	−12.275	−16.3333	−12.9778	−12.925	−19.0444
Desonide	−13.3444	−12.5111	−17.1667	−13.2833	−12.6222	−12.6286	−12.6778	−16.1889	−13.1	−12.7889	−17.3556
Rolitetracycline	−12.525	−12.4	−15.3778	−12.42	−12	−12.3	−13.225	−15.1111	−12.05	−12.0333	−17.4444
Metocurine	−14.1778	−12.5	−15.9	−12.3375	−12.2667	−13.4444	−13.5222	−15.4222	−13.4444	−12.5556	−19.3333
Drospirenone	−17.175	−12.8667	−17.25	−12.8857	−12.9778	−13.2556	−13.4222	−16.4889	−13.9111	−13.8444	−19.3333
Digitoxin	−12.7444	−12.9429	−14.25	−13.1444	−12.55	−12.2	−12.7625	−13.65	−12.6778	−12.6778	−16.6444
Danazol	−13.8143	−12.5	−15.9889	−12.45	−12.2667	−12.6333	−12.4	−13.975	−12.85	−12.775	−17.2111
Fusidic acid	−13.6778	−12.1	−15.2778	−12.4	−12.7	−12.1	−12.25	−15.0778	−12.5667	−12.3	−17.8111
Ixabepilone	−13.0111	−12.65	−17.4778	−13.1	−12.2	−12.8	−12.9222	−16.5222	−14.2667	−13.6333	−19.2333
Trabectedin	−16.5	−13.7556	−14.8875	−13.6	−12.6667	−12.95	−14.4556	−13.0778	−13.6111	−13.5667	−17.275
Abiraterone	−12.65	−12.55	−16.58	−12.45	−12.3	−12	−12.5	−14.7111	−12	−13.2111	−17.7111
Oxymetholone	−13.5375	−12.45	−16	−12.3	−12.4167	−12.6	−12.7833	−14.325	−12.7	−13.02	−17.1667
Stanozolol	−13.0625	−12.7	−15.7571	−12.2333	−12.56	−12.7667	−12.9833	−14.5889	−12.65	−12.92	−17.5
Eribulin	−16.3143	−13.1	−15.7222	−12.9333	−12.5667	−14.0222	−14.1444	−15.5667	−13.3111	−12.9556	−20.2444
flucloronide	−15.4714	−12.8778	−17.5667	−13.5	−13.4	−13.1333	−12.9667	−16.9667	−13.8556	−13.9889	−19.4889
Difluocortolone	−13.2444	−12.2	−15.8556	−12.3333	−12.24	−12.25	−12.32	−15.0889	−12.65	−12.5	−16.9222
Medrogestone	−13	−12.35	−16.6667	−12.6333	−12.3444	−12.3	−13.0667	−15.5778	−12.4556	−12.9778	−17.7222
Trypan blue free acid	−14.5333	−12.2833	−14.4556	−12.1667	−12.6	−12.425	−13.6556	−13.62	−12.4667	−13.0333	−17.6111
Fluprednisolone	−13.4889	−12.45	−16.0889	−12.56	−12.3444	−12.325	−12.6444	−14.9	−12.5	−12.7111	−17.2778
Rupatadine	−13.3333	−13	−16.3111	−12.75	−12.1	−12.9	−12.4	−15.7667	−12.3	−12.8667	−17.8889
Temoporfin	−13.9667	−13.7714	−14.5667	−13.9778	−12.3	−13.5778	−13.4556	−12.6	−13.4	−12.2833	−18.4
Clobetasol	−12.8556	−12.3	−15.3889	−12.275	−12.15	−12.1	−12.4	−14.4778	−12.6	−12.4333	−16.6111
Rifamycin	−13.7889	−12.2857	−15.7111	−12.6	−12.54	−14.2778	−13.7333	−15.5111	−12.9778	−13.125	−19.0111
Lurbinectedin	−14.7667	−13.7	−15.0125	−13.7778	−12.5571	−13.1	−14.7778	−15.3444	−13.4333	−13.6222	−17.0556
Lefamulin	−13.6222	−12.4	−15.8333	−12.4	−12.2	−12	−12.3333	−14.8222	−12.3778	−12.4	−17.5889
Methylprednisone	−13.9	−12.52	−16.5778	−12.5286	−12.5	−12.4333	−12.6	−15.3556	−12.6667	−13.0222	−17.5444
Glycyrrhizic acid	−14.9111	−14.8	−19.8	−13.6778	−13.8333	−12.1	−14.5	−18.45	−13.9778	−14.7	−19.7111
Fluticasone	−12.8333	−12.4833	−16.3556	−12.6714	−12.6429	−12.4	−12.1667	−15.6556	−12.3167	−12.5	−17.7556
Estradiol benzoate	−12.4667	−12.05	−16.7667	−12.2	−12.1	−12.4	−12.3	−14.5667	−12.4222	−12.5714	−17.5222
Hydrocortisone acetate	−13.4222	−12.5	−16.2667	−12.2	−12.3	−12.2333	−12.05	−14.3778	−12.45	−12.7333	−17.0111
Hydrocortisone phosphate	−12.85	−12.5	−15.8111	−12.15	−12.15	−12.375	−12.2	−14.75	−12.275	−12.52	−17.0222
Loteprednol	−12.9444	−12.2	−14.4333	−12.125	−12.1	−12.2	−12.7	−14.4444	−12.35	−13	−16.6333
Betamethasone phosphate	−12.8778	−12.7	−15.8333	−12.4	−12.45	−12.3167	−12	−14.2778	−12.3286	−12.2333	−17.3778
Benzhydrocodone	−12.5167	−12	−13.6444	−12.4	−12.3	−12.4	−12.15	−15	−12.3	−12.9667	−16.5667

Table 7
Repurposed drugs' characteristics.

Generic name	Structure	Current use	Mechanism of action	Side effects
Hydrocortisone	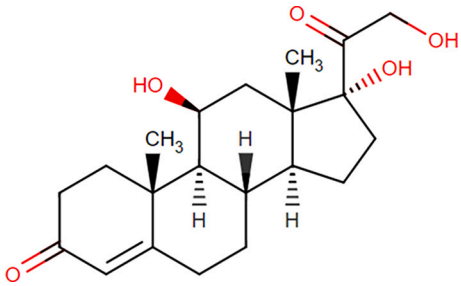	corticosteroid-responsive dermatoses, endocrine disorders, immune conditions, and allergic disorders	The short term effects of corticosteroids are decreased vasodilation and permeability of capillaries, as well as decreased leukocyte migration to sites of inflammation. [A187463] Corticosteroids binding to the glucocorticoid receptor mediates changes in gene expression that lead to multiple downstream effects over hours to days. [A187463] Glucocorticoids inhibit neutrophil apoptosis and demargination; they inhibit phospholipase A2, which decreases the formation of arachidonic acid derivatives; they inhibit NF-Kappa B and other inflammatory transcription factors; they promote anti-inflammatory genes like interleukin-10. [A187463] Lower doses of corticosteroids provide an anti-inflammatory effect, while higher doses are immunosuppressive. [A187463] High doses of glucocorticoids for an extended period bind to the mineralocorticoid receptor, raising sodium levels and decreasing potassium levels. [A187463]	Chronic high doses of glucocorticoids can lead to the development of cataract, glaucoma, hypertension, water retention, hyperlipidemia, peptic ulcer, pancreatitis, myopathy, osteoporosis, mood changes, psychosis, dermal atrophy, allergy, acne, hypertrichosis, immune suppression, decreased resistance to infection, moon face, hyperglycemia, hypocalcemia, hypophosphatemia, metabolic acidosis, growth suppression, and secondary adrenal insufficiency
Benzhydrocodone	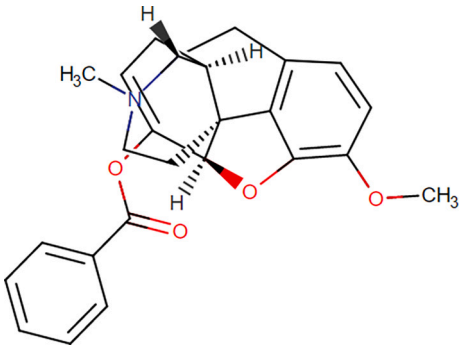	short-term management of acute pain requiring opioid therapy	Benzyhydrocodone is not reported to have pharmacological activity of its own and it not present in the plasma at detectable concentrations. Its active metabolite, hydrocodone is a mu-opioid receptor agonist.	Overdosage with benzhydrocodone presents as opioid intoxication including respiratory depression, somnolence, coma, skeletal muscle flaccidity, cold and clammy skin, constricted pupils, pulmonary edema, bradycardia, hypotension, partial or complete airway obstruction, atypical snoring, and death

need for further development of easily accessible drug interventions for treatment of symptomatic COVID-19 patients and to limit viral transmission. Repurposing of existing therapeutics presents the shortest path for drug development. Taken together, our integrative transcriptomics analysis was intended to identify DEGs and altered molecular pathways in different sources of human alveolar cells in response to SARS-CoV-2 infection. We identified 436 up-regulated genes enriched mainly in viral infectious disease, immune system, and signal transduction pathways. PPI network analysis of up-regulated protein coding genes revealed 44 hub genes. Up-regulated genes were also spotted in the published pathway of COVID-19 in KEGG and upstream proteins were identified. These target proteins (hub proteins and upstream proteins either to be inhibited or not) in response to SARS-CoV-2 infection were evaluated based on their contribution to viral respiratory diseases (i.e. MERS, SARS, Influenza A, Measles, Hepatitis B and C) and main inflammatory pathways (i.e. TNF, IL-17, NF-kB, and TLR signaling pathways as well as rheumatoid arthritis). Grouped into pro- and anti-viral proteins, the former (ADAR, HBEGF, MMP9, USP18, JUN, FOS, IRF2, ICAM1, IFI35, CASP1, and STAT3) is mainly involved in inflammatory responses whose inhibition may provide some perspectives into the COVID-19 management attempts. Through docking all FDA-approved drugs with pro- and anti-viral proteins, Hydrocortisone and Benzhydrocodone were suggested as repurposed drugs which should be investigated thoroughly in terms of efficacy via wet-lab experiments followed by clinical studies.

Funding

This work was supported by the Deputy of Research and Technology, Golestan University of Medical Sciences [grant number: 111497].

CRediT authorship contribution statement

SeyedehMozhdeh Mirmohammadi: Conceptualization, Data curation, Formal analysis, Investigation, Methodology, Software, Supervision, Writing – original draft. **Anvarsadat Kianmehr:** Funding acquisition, Project administration, Data curation, Formal analysis, Investigation, Methodology, Supervision, Visualization, Writing – original draft, Writing – review & editing. **Amir Sabbaghian:** Data curation, Formal analysis, Investigation, Software, Visualization. **Alireza Mohebbi:** Data curation, Investigation, Methodology, Software, Supervision. **Hamid Shahbazmohammadi:** Conceptualization, Investigation,

Software, Visualization. **Mehdi Sheykharabi:** Conceptualization, Methodology, Supervision. **Zahra Bazzi:** Conceptualization, Methodology.

Declaration of Competing Interest

None.

Acknowledgments

We express our gratitude to Infectious Diseases Research Center, Golestan University of Medical Sciences.

Appendix A. Supplementary data

Supplementary data to this article can be found online at https://doi.org/10.1016/j.meegid.2022.105318.

References

Balajelini, M., Mohammad, Al Vakili, Rajabi, A., Mohammadi, M., Tabarraei, A., Hosseini, S.M., 2020. Recovery of Olfactory and Gustatory Dysfunctions in COVID-19 Patients in Iran: A Prospective Cohort Study. https://doi.org/10.21203/rs.3.rs-132300/v1.

Barrett, T., Wilhite, S.E., Ledoux, P., Evangelista, C., Kim, I.F., Tomashevsky, M., Marshall, K.A., Phillippy, K.H., Sherman, P.M., Holko, M., Yefanov, A., Lee, H., Zhang, N., Robertson, C.L., Serova, N., Davis, S., Soboleva, A., 2013. NCBI GEO: archive for functional genomics data sets–update. Nucleic Acids Res. 41, D991–D995. https://doi.org/10.1093/nar/gks1193.

Bizzotto, J., Sanchis, P., Abbate, M., Lage-Vickers, S., Lavignolle, R., Toro, A., Olszevicki, S., Sabater, A., Cascardo, F., Vazquez, E., Cotignola, J., Gueron, G., 2020. SARS-CoV-2 infection boosts MX1 antiviral effector in COVID-19 patients. iScience 23, 101585. https://doi.org/10.1016/j.isci.2020.101585.

Blanco-Melo, D., Nilsson-Payant, B.E., Liu, W.-C., Uhl, S., Hoagland, D., Møller, R., Jordan, T.X., Oishi, K., Panis, M., Sachs, D., Wang, T.T., Schwartz, R.E., Lim, J.K., Albrecht, R.A., tenOever, B.R., 2020. Imbalanced host response to SARS-CoV-2 drives development of COVID-19. Cell 181, 1036–1045.e9. https://doi.org/10.1016/j.cell.2020.04.026.

Catanzaro, M., Fagiani, F., Racchi, M., Corsini, E., Govoni, S., Lanni, C., 2020. Immune response in COVID-19: addressing a pharmacological challenge by targeting pathways triggered by SARS-CoV-2. Signal Transduct. Target. Ther. https://doi.org/10.1038/s41392-020-0191-1.

Chen, E.Y., Tan, C.M., Kou, Y., Duan, Q., Wang, Z., Meirelles, G.V., Clark, N.R., Ma'ayan, A., 2013. Enrichr: interactive and collaborative HTML5 gene list enrichment analysis tool. BMC Bioinformatics 14, 128. https://doi.org/10.1186/1471-2105-14-128.

Galani, I.-E., Rovina, N., Lampropoulou, V., Triantafyllia, V., Manioudaki, M., Pavlos, E., Koukaki, E., Fragkou, P.C., Panou, V., Rapti, V., Koltsida, O., Mentis, A., Koulouris, N., Tsiodras, S., Koutsoukou, A., Andreakos, E., 2021. Untuned antiviral immunity in COVID-19 revealed by temporal type I/III interferon patterns and flu comparison. Nat. Immunol. 22, 32–40. https://doi.org/10.1038/s41590-020-00840-x.

Gélinas, J.-F., Clerzius, G., Shaw, E., Gatignol, A., 2011. Enhancement of replication of RNA viruses by ADAR1 via RNA editing and inhibition of RNA-activated protein kinase. J. Virol. 85, 8460–8466. https://doi.org/10.1128/JVI.00240-11.

Hazra, S., Chaudhuri, A.G., Tiwary, B.K., Chakrabarti, N., 2020. Matrix metallopeptidase 9 as a host protein target of chloroquine and melatonin for immunoregulation in COVID-19: a network-based meta-analysis. Life Sci. 257, 118096 https://doi.org/10.1016/j.lfs.2020.118096.

Herold, S., Becker, C., Ridge, K.M., Budinger, G.R.S., 2015. Influenza virus-induced lung injury: pathogenesis and implications for treatment. Eur. Respir. J. 45, 1463–1478. https://doi.org/10.1183/09031936.00186214.

Jin, Y., Ji, W., Yang, H., Chen, S., Zhang, W., Duan, G., 2020. Endothelial activation and dysfunction in COVID-19: from basic mechanisms to potential therapeutic approaches. Signal Transduct. Target. Ther. 5, 293. https://doi.org/10.1038/s41392-020-00454-7.

Källberg, M., Wang, H., Wang, S., Peng, J., Wang, Z., Lu, H., Xu, J., 2012. Template-based protein structure modeling using the RaptorX web server. Nat. Protoc. 7, 1511–1522. https://doi.org/10.1038/nprot.2012.085.

Kanehisa, M., Sato, Y., 2020. KEGG mapper for inferring cellular functions from protein sequences. Protein Sci. 29, 28–35. https://doi.org/10.1002/pro.3711.

Kim, J.-H., Luo, J.-K., Zhang, D.-E., 2008. The level of hepatitis B virus replication is not affected by protein ISG15 modification but is reduced by inhibition of UBP43 (USP18) expression. J. Immunol. 181, 6467–6472. https://doi.org/10.4049/jimmunol.181.9.6467.

Kuleshov, M.V., Jones, M.R., Rouillard, A.D., Fernandez, N.F., Duan, Q., Wang, Z., Koplev, S., Jenkins, S.L., Jagodnik, K.M., Lachmann, A., McDermott, M.G., Monteiro, C.D., Gundersen, G.W., Ma'ayan, A., 2016. Enrichr: a comprehensive gene set enrichment analysis web server 2016 update. Nucleic Acids Res. 44, W90–W97. https://doi.org/10.1093/nar/gkw377.

Kurokawa, C., Iankov, I.D., Galanis, E., 2019. A key anti-viral protein, RSAD2/VIPERIN, restricts the release of measles virus from infected cells. Virus Res. 263, 145–150. https://doi.org/10.1016/j.virusres.2019.01.014.

Le Goffic, R., Pothlichet, J., Vitour, D., Fujita, T., Meurs, E., Chignard, M., Si-Tahar, M., 2007. Cutting edge: influenza A virus activates TLR3-dependent inflammatory and RIG-I-dependent antiviral responses in human lung epithelial cells. J. Immunol. 178, 3368–3372. https://doi.org/10.4049/jimmunol.178.6.3368.

Lee, J.S., Shin, E.-C., 2020. The type I interferon response in COVID-19: implications for treatment. Nat. Rev. Immunol. 20, 585–586. https://doi.org/10.1038/s41577-020-00429-3.

Lei, X., Dong, X., Ma, R., Wang, W., Xiao, X., Tian, Z., Wang, C., Wang, Y., Li, L., Ren, L., Guo, F., Zhao, Z., Zhou, Z., Xiang, Z., Wang, J., 2020. Activation and evasion of type I interferon responses by SARS-CoV-2. Nat. Commun. 11, 1–12. https://doi.org/10.1038/s41467-020-17665-9.

Lindner, H.A., Lytvyn, V., Qi, H., Lachance, P., Ziomek, E., Ménard, R., 2007. Selectivity in ISG15 and ubiquitin recognition by the SARS coronavirus papain-like protease. Arch. Biochem. Biophys. 466, 8–14. https://doi.org/10.1016/j.abb.2007.07.006.

Loganathan, T., Ramachandran, S., Shankaran, P., Nagarajan, D., Suma Mohan, S., 2020. Host transcriptome-guided drug repurposing for COVID-19 treatment: a meta-analysis based approach. PeerJ 2020, 1–27. https://doi.org/10.7717/peerj.9357.

Maddah, S.A., Modanloo, M., 2020. The challenges of keeping psychiatric patients safe in rehabilitation centers during coronavirus outbreak. Arch. Psychiatr. Nurs. 34, 580–581. https://doi.org/10.1016/j.apnu.2020.07.024.

Mckechnie, J.L., Blish, C.A., 2020. The Innate Immune System: Fighting on the Front Lines or Fanning the Flames of COVID-19, pp. 863–869. https://doi.org/10.1016/j.chom.2020.05.009.

Mirmohammadi, S., Kianmehr, A., Arefi, M., Mahrooz, A., 2020. Biochemical parameters and pathogenesis of SARS-CoV-2 infection in vital organs: COVID-19 outbreak in Iran. New microbes new Infect. 38, 100792 https://doi.org/10.1016/j.nmni.2020.100792.

Mokhtari, T., Hassani, F., Ghaffari, N., Ebrahimi, B., Yarahmadi, A., 2020. COVID-19 and multiorgan failure: a narrative review on potential mechanisms. J. Mol. Histol. 51, 613–628. https://doi.org/10.1007/s10735-020-09915-3.

Nagashima, S., Mendes, M.C., Camargo Martins, A.P., Borges, N.H., Godoy, T.M., Miggiolaro, A.F.R.D.S., da Silva Dezidério, F., Machado-Souza, C., de Noronha, L., 2020. Endothelial dysfunction and thrombosis in patients with COVID-19-brief report. Arterioscler. Thromb. Vasc. Biol. 40, 2404–2407. https://doi.org/10.1161/ATVBAHA.120.314860.

Ortiz-prado, E., Simbaña-rivera, K., Barreno, L.G., Rubio-neira, M., Guaman, L.P., Kyriakidis, N.C., Muslin, C., María, A., Jaramillo, G., Barba-ostria, C., Cevallos-robalino, D., Sanches-sanmiguel, H., Unigarro, L., Zalakeviciute, R., Gadian, N., López-cortés, A., 2020. Clinical, Molecular, and Epidemiological Characterization of the SARS-CoV-2 Virus and the Coronavirus Disease 2019 (COVID-19), A Comprehensive Literature Review, 98. https://doi.org/10.1016/j.diagmicrobio.2020.115094.

Park, A., Iwasaki, A., 2020. Type I and type III interferons-induction, signaling, evasion, and application to combat COVID-19. Cell Host Microbe 27, 870–878. https://doi.org/10.1016/j.chom.2020.05.008.

Quintero, P.A., Knolle, M.D., Cala, L.F., Zhuang, Y., Owen, C.A., 2010. Matrix metalloproteinase-8 inactivates macrophage inflammatory protein-1 alpha to reduce acute lung inflammation and injury in mice. J. Immunol. 184, 1575–1588. https://doi.org/10.4049/jimmunol.0900290.

Ribero, M.S., Jouvenet, N., Dreux, M., Nisole, S., 2020. Interplay between SARS-CoV-2 and the type I interferon response. PLoS Pathog. 16, 1–22. https://doi.org/10.1371/journal.ppat.1008737.

Ritchie, K.J., Hahn, C.S., Kim, K. Il, Yan, M., Rosario, D., Li, L., de la Torre, J.C., Zhang, D.-E., 2004. Role of ISG15 protease UBP43 (USP18) in innate immunity to viral infection. Nat. Med. 10, 1374–1378. https://doi.org/10.1038/nm1133.

Rojas-Quintero, J., Wang, X., Tipper, J., Burkett, P.R., Zuñiga, J., Ashtekar, A.R., Polverino, F., Rout, A., Yambayev, I., Hernández, C., Jimenez, L., Ramírez, G., Harrod, K.S., Owen, C.A., 2018. Matrix metalloproteinase-9 deficiency protects mice from severe influenza A viral infection. JCI insight 3. https://doi.org/10.1172/jci.insight.99022.

Samuel, C.E., 2001. Antiviral actions of interferons. Clin. Microbiol. Rev. 14, 778–809. Table of contents. https://doi.org/10.1128/CMR.14.4.778-809.2001.

Shannon, P., Markiel, A., Ozier, O., Baliga, N.S., Wang, J.T., Ramage, D., Amin, N., Schwikowski, B., Ideker, T., 2003. Cytoscape: a software environment for integrated models of biomolecular interaction networks. Genome Res. 13, 2498–2504. https://doi.org/10.1101/gr.1239303.

Shi, Y., Wang, Y., Shao, C., Huang, J., Gan, J., Huang, X., Bucci, E., Piacentini, M., Ippolito, G., Melino, G., 2020. COVID-19 infection: the perspectives on immune responses. Cell Death Differ. https://doi.org/10.1038/s41418-020-0530-3.

Swaim, C.D., Canadeo, L.A., Monte, K.J., Khanna, S., Lenschow, D.J., Huibregtse, J.M., 2020. Modulation of extracellular ISG15 signaling by pathogens and viral effector proteins. Cell Rep. 31, 107772 https://doi.org/10.1016/j.celrep.2020.107772.

Szklarczyk, D., Gable, A.L., Lyon, D., Junge, A., Wyder, S., Huerta-Cepas, J., Simonovic, M., Doncheva, N.T., Morris, J.H., Bork, P., Jensen, L.J., von Mering, C., 2019. STRING v11: protein–protein association networks with increased coverage, supporting functional discovery in genome-wide experimental datasets. Nucleic Acids Res. 47, D607–D613. https://doi.org/10.1093/nar/gky1131.

Trott, O., Olson, A.J., 2010. AutoDock Vina: improving the speed and accuracy of docking with a new scoring function, efficient optimization, and multithreading. J. Comput. Chem. 31, 455–461. https://doi.org/10.1002/jcc.21334.

Tufan, A., Avanoğlu Güler, A., Matucci-Cerinic, M., 2020. COVID-19, immune system response, hyperinflammation and repurposing antirheumatic drugs. Turkish J. Med. Sci. 50, 620–632. https://doi.org/10.3906/sag-2004-168.

Vanderheiden, A., Ralfs, P., Chirkova, T., Upadhyay, A.A., Zimmerman, M.G., Bedoya, S., Aoued, H., Tharp, G.M., Pellegrini, K.L., Manfredi, C., Sorscher, E., Mainou, B., Lobby, J.L., Kohlmeier, J.E., Lowen, A.C., Shi, P.-Y., Menachery, V.D., Anderson, L. J., Grakoui, A., Bosinger, S.E., Suthar, M.S., 2020. Type I and type III interferons restrict SARS-CoV-2 infection of human airway epithelial cultures. J. Virol. 94 https://doi.org/10.1128/JVI.00985-20.

Venkataraman, T., Frieman, M.B., 2017. The role of epidermal growth factor receptor (EGFR) signaling in SARS coronavirus-induced pulmonary fibrosis. Antivir. Res. 143, 142–150. https://doi.org/10.1016/j.antiviral.2017.03.022.

Venkataraman, T., Coleman, C.M., Frieman, M.B., 2017. Overactive epidermal growth factor receptor signaling leads to increased fibrosis after severe acute respiratory syndrome coronavirus infection. J. Virol. 91 https://doi.org/10.1128/JVI.00182-17.

Verhelst, J., Parthoens, E., Schepens, B., Fiers, W., Saelens, X., 2012. Interferon-inducible protein Mx1 inhibits influenza virus by interfering with functional viral ribonucleoprotein complex assembly. J. Virol. 86, 13445–13455. https://doi.org/10.1128/JVI.01682-12.

Villeret, B., Solhonne, B., Straube, M., Lemaire, F., Cazes, A., Garcia-Verdugo, I., Sallenave, J.-M., 2020. Influenza A virus pre-infection exacerbates *Pseudomonas aeruginosa*-mediated lung damage through increased MMP-9 expression, decreased Elafin production and tissue resilience. Front. Immunol. 11, 117. https://doi.org/10.3389/fimmu.2020.00117.

Yoshizaki, T., Sato, H., Furukawa, M., Pagano, J.S., 1998. The expression of matrix metalloproteinase 9 is enhanced by Epstein-Barr virus latent membrane protein 1. Proc. Natl. Acad. Sci. U. S. A. 95, 3621–3626. https://doi.org/10.1073/pnas.95.7.3621.

Zhou, Z., Ren, L., Zhang, L., Zhong, J., Xiao, Y., Jia, Z., Guo, L., Yang, Jing, Wang, C., Jiang, S., Yang, D., Zhang, G., Li, H., Chen, F., Xu, Y., Chen, M., Gao, Z., Yang, Jian, Dong, J., Liu, B., Zhang, X., Wang, W., He, K., Jin, Q., Li, M., Wang, J., 2020. Heightened innate immune responses in the respiratory tract of COVID-19 patients. Cell Host Microbe 27, 883–890.e2. https://doi.org/10.1016/j.chom.2020.04.017.